REVIEW OF SCIENTIFIC INSTRUMENTS **89**, 053302 (2018)

Source-to-accelerator quadrupole matching section for a compact linear accelerator

P. A. Seidl,[1,a)] A. Persaud,[1] W. Ghiorso,[1] Q. Ji,[1] W. L. Waldron,[1] A. Lal,[2] K. B. Vinayakumar,[2] and T. Schenkel[1]

[1]*Ernest Orlando Lawrence Berkeley National Laboratory, 1 Cyclotron Road, Berkeley, California 94720, USA*
[2]*SonicMEMS Laboratory, Cornell University, Ithaca, New York 14853, USA*

(Received 23 January 2018; accepted 23 April 2018; published online 11 May 2018)

Recently, we presented a new approach for a compact radio-frequency (RF) accelerator structure and demonstrated the functionality of the individual components: acceleration units and focusing elements. In this paper, we combine these units to form a working accelerator structure: a matching section between the ion source extraction grids and the RF-acceleration unit and electrostatic focusing quadrupoles between successive acceleration units. The matching section consists of six electrostatic quadrupoles (ESQs) fabricated using 3D-printing techniques. The matching section enables us to capture more beam current and to match the beam envelope to conditions for stable transport in an acceleration lattice. We present data from an integrated accelerator consisting of the source, matching section, and an ESQ doublet sandwiched between two RF-acceleration units. *Published by AIP Publishing.* https://doi.org/10.1063/1.5023415

I. INTRODUCTION

In 2017, we presented a new approach to enable compact RF particle accelerators for the generation of high intensity ion beams.[1,2] Using fabrication techniques used in the computer industry, the dimensions of the focusing and acceleration electrodes are reduced to the mm-scale, much smaller than conventional particle accelerators. The concept was motivated by research from the 1970s and 1980s on the acceleration of many parallel beams for heavy ion-driven inertial fusion energy. This earlier work showed that for these unusually high beam current requirements (hundreds of amperes to kiloamperes), the considerable space charge could be feasibly managed by accelerating many closely spaced lower current beams more economically than a small number of beams in separate accelerator structures.[3,4]

Focusing and acceleration fields are limited by electrical breakdown, and for a quadrupole focusing element, a maximum operating field on the electrode will produce a stronger focusing gradient in a smaller diameter channel. Maschke[3,4] showed that as the multiple-beam electrostatic focusing electrodes and apertures are scaled to smaller dimensions, the average current density scales favorably and increases until alignment tolerances and vacuum pressure in the dense structure lead to excessive emittance growth and beam loss. Building on Maschke's work, experiments by Urbanus *et al.*, with a prototype multiple-beam RF accelerator, demonstrated[5] the concept for a beam-beam separation of 1.3 cm. Similarly, others were motivated to address high-space charge with closely packed quadrupole focusing arrays in a common induction accelerator for heavy ion inertial fusion energy[6] using electrostatic and magnetic focusing quadrupoles.

Recent developments of micro-electromechanical systems (MEMS) have demonstrated impressive fabrication tolerances at very low cost, presenting a path forward to mm-scale, densely packed beams with electrostatic focusing and RF acceleration. Our first results with mm-scale structures are described in Refs. 1 and 2.

Scaling to a large number of densely packed beams may lead to various applications, such as mass analysis for ion implantation (few mA and up to 300 keV ion energy).[7] At higher current per beam, with each beam approaching the focusing limits set by space charge repulsion and beam loading in the RF system, the compact accelerator may meet the extreme beam requirements for ion beam heating of plasmas for fusion energy applications.[8]

In this paper, we address the challenge of the transverse matching of many round beams from the ion source to the alternating-gradient focusing channels of the accelerator. We then carry out an integrated test of a working accelerator structure, including the matching section between the ion source extraction grids, RF-acceleration sections, and electrostatic focusing quadrupoles between adjacent acceleration units.

II. MATCHING SECTION DESIGN

Beams injected from ion sources are usually cylindrically symmetric in profile and may be slightly converging or diverging depending on the ion optics in the injector and the beam properties such as emittance and space charge. For injection into accelerators with alternating-gradient quadrupole focusing systems, the matched beam conditions midway between quadrupoles are generally a cylindrically symmetric spatial profile (x-y space), but the beam is often converging in one plane and diverging in the other. This may be seen from the

a)Electronic mail: paseidl@lbl.gov

solutions to the rms envelope equation for an alternating gradient quadrupole focusing lattice.[9,10] To minimize particle loss and emittance growth, a special matching section of several quadrupoles is often used to transform the beam envelope from the round conditions at the exit of the injector to matched beam conditions in the accelerator lattice.

The transverse envelope equations describe the rms beam size as a function of the propagation direction subject to the applied electrostatic focusing fields from the quadrupoles, the effective defocusing due to the beam emittance, and the defocusing self-field of the ion beam. In the absence of field imperfections (non-quadrupole moments in the x–y plane), the system has four-fold symmetry and the horizontal and vertical equations are coupled via the space charge term,

$$a'' = \kappa a + \frac{\epsilon^2}{a^3} + \frac{2K}{a+b} \tag{1}$$

and

$$b'' = -\kappa b + \frac{\epsilon^2}{b^3} + \frac{2K}{a+b}. \tag{2}$$

The derivatives are with respect to the beam propagation axis (z), and a and b are the horizontal and vertical 2·*rms* envelope coordinates of the beam envelope. The quadrupole focusing strength, 4·*rms* un-normalized emittance, and dimensionless perveance of the beam are denoted by κ, ϵ, and K, respectively. For non-relativistic particles, the dimensionless perveance is

$$K = \frac{\lambda_q}{4\pi\epsilon_0 V_b}, \tag{3}$$

and the focusing constant is

$$\kappa = \frac{V}{V_b R^2}, \tag{4}$$

where λ_q is the linear charge density of the ion beam, V is the quadrupole potential, R is the radius from the aperture center to the electrode, and V_b is the beam voltage. The beam envelope is simulated via numerical integration of the envelope equations, initialized by the beam parameters (a_i, a_i', b_i, and b_i') at the exit of the injector. These parameters were measured by imaging the beam profile at two axial locations downstream of the injector (without the matching section). A minimum of four quadrupoles is needed to solve for the quadrupole focusing strengths to match the beam envelope to the periodic focusing solution of the downstream elements, $a(z) = a(z + L)$, where L is the lattice period of the quadrupole focusing lattice in the accelerator and similarly for a_i', b_i, and b_i'. For these first experiments with the matching section, we chose solutions to establish a simpler, converging beam at the entrance to the accelerator. Figure 1 shows a solution which transforms the axi-symmetric diverging beam at the exit of the injector to a converging beam downstream of the matching section with a similar beam radius. To achieve this, we have used a FDDFFD solution instead of an alternating gradient pattern between focusing (F) and defocusing (D) in a given plane between successive quadrupoles (FDFD. . .).

The input beam parameters are shown in Table I, and the quadrupole voltages are all less than 600 V to be established in a bipolar manner. The relevant source quantities are based in

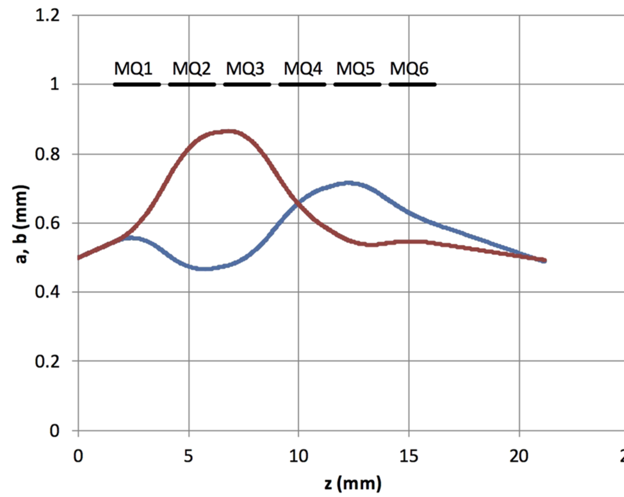

FIG. 1. An example RMS envelope solution for a single beam. The assumed initial conditions of the beam are based on an average measurement of the beam envelope at the exit of the injector. The quadrupole voltages are chosen to establish a converging beam condition at the entrance of the accelerator section immediately downstream of the six-quadrupole matching section. The horizontal lines indicate the length and positions of the quadrupole apertures.

TABLE I. Beam parameters and quadrupole voltages for the simulation in Fig. 1.

a_i (mm)	0.5	V_1 (V)	552
a_i' (rad)	0.028	V_2 (V)	−500
ϵ (mm)	6.3×10^{-4}	V_3 (V)	−512
E_{ion} (keV)	8.0	V_4 (V)	359
Mass (amu)	40	V_5 (V)	352
		V_6 (V)	−136

part on measurements and plasma source simulations. Beam profile measurements at two drift distances determined the beam divergence angle. IGUN simulations[11] modeled the positive ion extraction from the plasma and the resulting emittance of the single beams exiting the multi-aperture grid structure. The beam current values are close to those in the experiment, measured directly downstream of the ion source. The solution is for an 8 keV Ar^+ ion beam (I = 7 μA, ϵ = 0.63 μm). However, the quadrupole voltage solution is insensitive to the ion mass species and can transport a variety of ion species without extensive retuning. An envelope solution that establishes matched conditions at the beginning of an accelerator section is shown in Fig. 2.

III. QUADRUPOLE FABRICATION AND EXPERIMENTAL SETUP

The principal components of the mechanical assembly are the electrodes which when electrically biased define the quadrupole field pattern and the support frames which support the electrodes and maintain overall alignment. The electrodes are electroless nickel-coated on a monomer resin substrate.[12] The substrates were manufactured with a rapid prototype, 3D-printing process, leading to the high precision (25 μm) needed to maintain the electrode shapes and spacings for

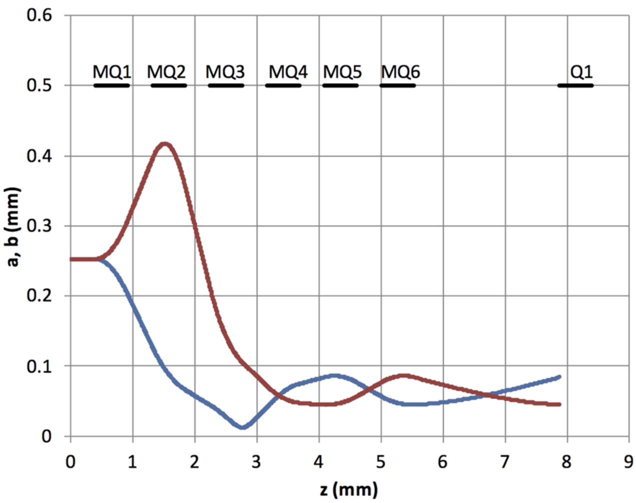

FIG. 2. Matched beam solution for a more compact structure, with 1-mm diameter apertures.

good alignment and field quality with low component cost. The electrode components are held in polyether ether ketone (PEEK) plastic support frames. Since this is a multiple-beam structure, each polarity electrode for a quadrupole array is supported by connecting ribs to enable close spacing, as shown in Fig. 3.

One set of electrodes overlays the opposing polarity electrodes, and they fully overlap in z forming a quadrupole of length 2 mm with gaps of 0.5 mm between successive quadrupoles. Electrical continuity to the electrodes is via soldered connections to a vapor-deposited gold coating on the PEEK supports, which in turn contacts the nickel-coated quadrupole electrodes. The nickel coating process slightly warped the quadrupole electrode parts ($\approx$1 mm across the 40-mm^2). However, when held at the perimeter by the more rigid PEEK holders, the electrodes were restored to the desired coplanar orientation. A coordinate measuring survey of the assembly showed beam-center spacing (pitch between beams: 5.0 mm) errors and electrode diameter errors well within the 25 μm tolerance specifications. The computer aided design

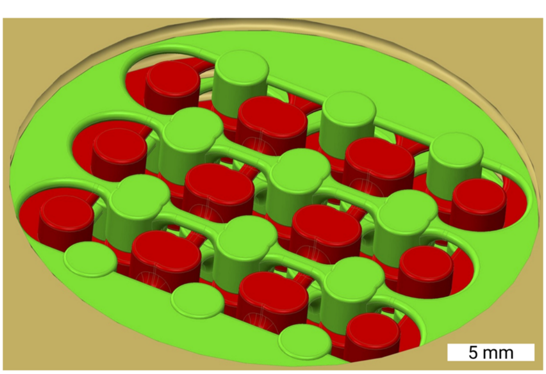

FIG. 3. The CAD model shows the cylindrical electrodes (red and green) supported by thin ribs. Each electrode part holds all the electrodes for one polarity of the nine-beam array and is held in place by an outer plastic holder (brown). The ribs provide mechanical support and electrical connection to the DC power supplies. The centers of beamline axes are separated by 5 mm in the rectangular array.

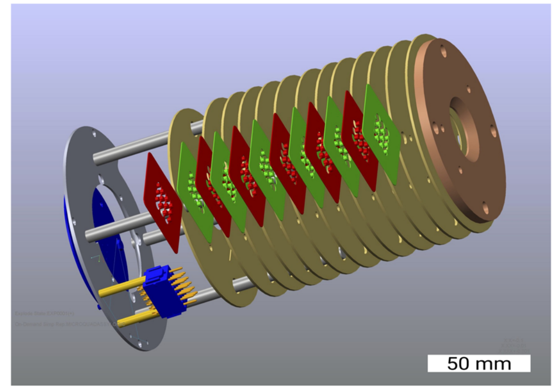

FIG. 4. The CAD model of the quadrupole assembly is shown in an exploded view for clarity. The quadrupole electrodes (highlighted in red and green) are supported within the larger plastic (PEEK) holders. The holders are in turn held in alignment by stainless steel rods mounted to a base plate.

of the model of the assembly is shown in Fig. 4, illustrating that a 3×3 transverse array of quadrupoles is comprised of a pair of electrode parts where one part (green) will be biased to, e.g., $+V$ for the horizontally oriented electrodes and the vertically oriented electrodes (red) are biased to $-V$. Thus, the voltages that establish a particular matching solution are common to all nine beams.

The assembled matching section is shown in Fig. 5. Note that there is considerable radial space available within this footprint to build a quadrupole array with many more beams,

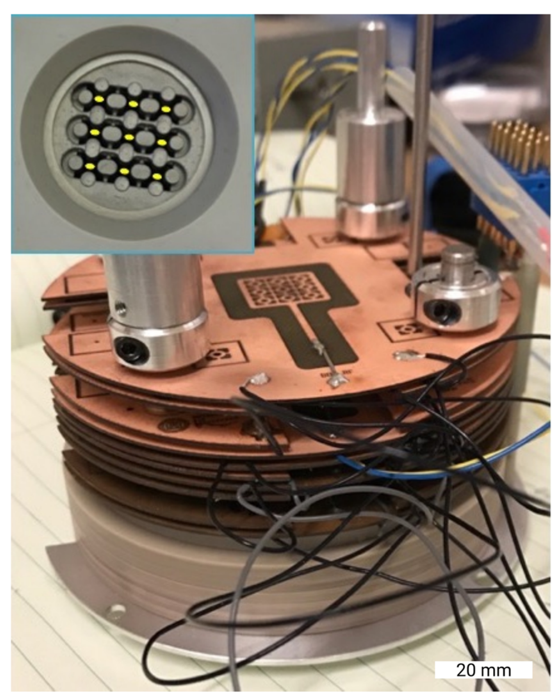

FIG. 5. The photograph of the final assembly shows the most downstream matching quadrupole (inset) within the outer support structure. The beams are represented schematically by the yellow ellipses. In the main photo, the matching section is at the bottom of the assembly, and only the plastic supports are visible. The RF accelerator section, fabricated from laser-cut, 10-cm diameter printed-circuit boards is aligned via the common alignment rods at gaps between the elements that are set to match the RF frequency and ion velocity.

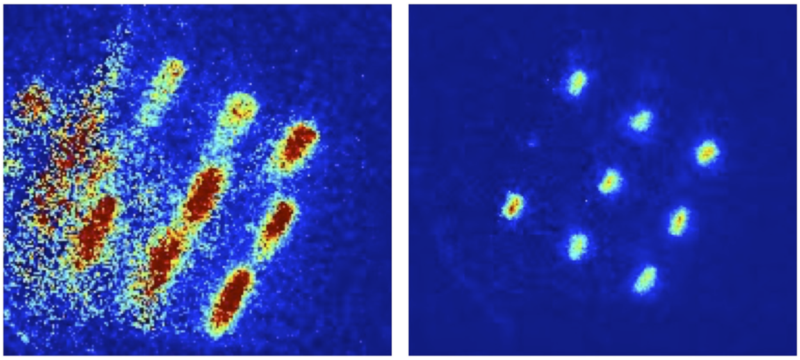

FIG. 6. Left: Normalized scintillator beam image for only the first matching quadrupole energized showing the typical focusing/defocusing effects of a quadrupoles. Right: Normalized scintillator image when all quadrupoles are energized showing tightly focused beams. Beamlet-to-beamlet variations and noise in the image are due to background light variation and do not represent beam fluctuations.

which would transmit a higher overall beam current, depending quadratically on the array size.

In the previous work,[1] we demonstrated the acceleration of ion beams through four acceleration gaps and quadrupole focusing through a pair of electrostatic quadrupoles.[2] In this work, we began by installing only the matching section downstream of the injector. The filament-driven RF Ar^+ source with a 3 × 3 array of extraction electrodes injected ions to the matching section.[13] The exiting beam was diagnosed with an Al_2O_3 scintillator and image-intensified CCD camera. Following these observations, the RF accelerator section was added downstream of the matching section, with four acceleration gaps and two quadrupoles. The quadrupole and RF acceleration electrodes are fabricated from laser-cut, copper-clad PC-boards. The radius of the quadrupole and RF electrode apertures is 1 mm, half the matching section aperture.

IV. RESULTS AND DISCUSSION

Each quadrupole was first energized separately, and the expected elliptical beam pattern was observed in accordance with the quadrupole polarity setting. Figure 6 shows an example for the first matching quadrupole energized where the focusing/defocusing effect is clearly visible despite some background light in the image. When all the quadrupoles are energized, the beams are tightly focused as can be seen in the right image of Fig. 6 (the variation in amplitude for each beamlet is due to background correction and does not represent beam current variation).

The ion source was pulsed for 1.5 ms, generating a nearly constant current during the pulse. Figure 7 shows that the transmitted beam current was approximately 2× greater with the matching section energized. When the matching section is energized, the total current is equal to that in the previous work without a matching section[1] where the beams traversed fewer wafers than in this experiment. There, the round beams were injected directly into the acceleration wafers without any focusing quadrupoles. The equality between our previous work and this experiment is fortuitous—clearly it is not expected to hold for many more acceleration stages in the absence of transverse focusing with well-controlled envelope parameters. The results here show the transport of the beams without loss through the accelerator and the simultaneous control of the envelope parameters to match conditions needed for stable transverse focusing and control (less beam loss) over many more lattice periods.

We demonstrated the operation of the integrated assembly, including RF acceleration and quadrupole focusing in the acceleration section as shown in Fig. 8. The RF acceleration electrodes were driven from a common RF amplifier. The spacing between successive acceleration gaps was set to $\beta\lambda/2$, as is common in RF accelerators, where $\beta = v/c$ and $\lambda = c/f$, the RF wavelength. Thus particles near the peak of the acceleration waveform are subject to the same acceleration field at each gap.

The retarding potential of the decelerating grid was varied within the range $8 \leq V_g \leq 14$ kV, and the injected ion energy was $E_i = 11$ keV. Since the RF frequency was 15 MHz, the relatively long beam pulses span many RF oscillations. Consequently, ions out of phase with the peak accelerating part of the RF waveform received less acceleration or were decelerated, and a continuum of ion energies is produced between $E_i - \delta E$ and $E_i + \delta E$. Argon ion energies up to 13 keV were detected through the four acceleration gaps for 1.5 ms duration pulses, as shown in Fig. 9. Extrapolating to many more acceleration gaps, the slower ions would be further out of phase and eventually lost, and the higher energy ions would be preferentially transported and accelerated.

Some voltage-breakdown in the matching section was observed. Contributing factors are secondary-electrons from ions striking the electrodes and nearby insulators. This will be remedied by tuning the envelope solution. Also, the matching section has a rather closed geometry, and we will add side-vents with higher pumping conductance to achieve a lower pressure within the matching section.

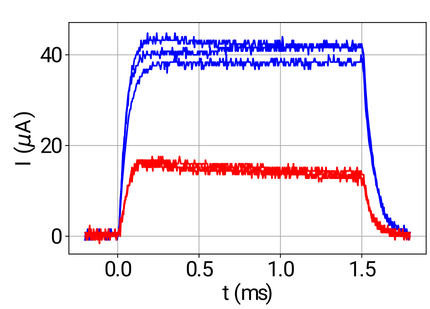

FIG. 7. The beam current detected by the Faraday cup downstream of the accelerator section shows approximately 2× more current with the matching section on (blue) vs off (red). Three ion pulses are shown for each case.

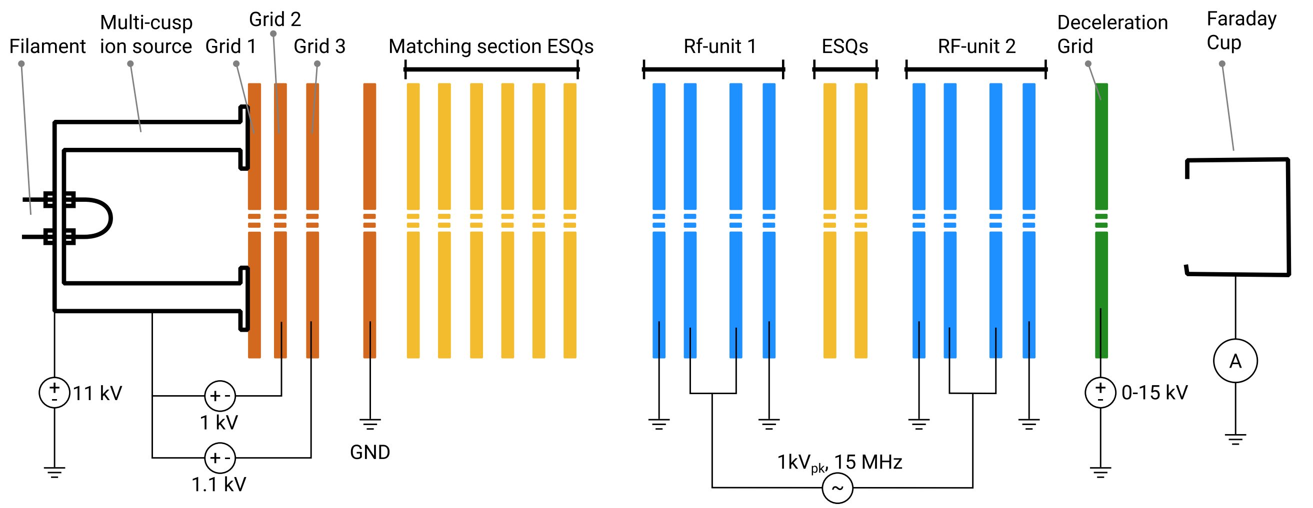

FIG. 8. Schematic of the experiment. An argon plasma is generated in the multi-cusp ion source which floats at 11 kV. Ions are extracted through an aligned 3 × 3 hole plate assembly (grids) to ground potential and injected into the matching quadrupoles. For the first measurements, the ion beam distribution was characterized by a scintillator after the matching section. In subsequent measurements with an integrated system, the accelerator section (four RF acceleration gaps and two quadrupoles) was added as shown. A Faraday cup detected the transmitted ion current.

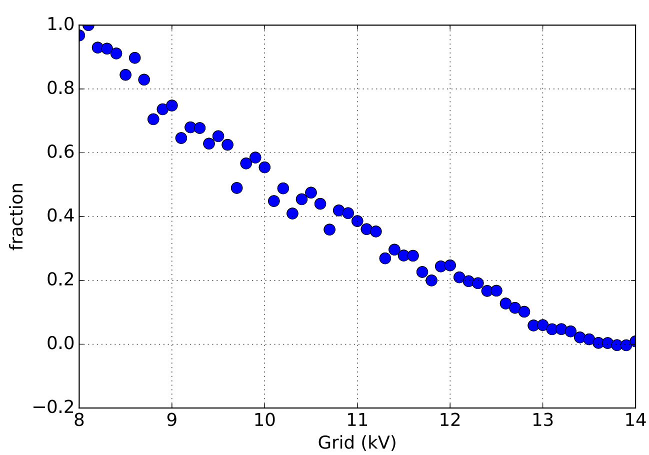

FIG. 9. The retarding grid scan shows the fraction of transmitted current as a function of the retarding grid potential. The results show acceleration >2 keV above the injection energy of 11 keV indicating a RF acceleration voltage of >0.5 kV/gap.

V. CONCLUSION AND OUTLOOK

We have fabricated a compact, multiple-beam quadrupole matching system to transform the round beams exiting a multiple-beam ion-source to the parameters required for high transmission of ions in an alternating gradient focusing system of an RF accelerator. The electrode structure substrates are 3D-printed monomer resins with nickel coating to define the quadrupole electrostatic fields, and parallel beams have a center-to-center spacing of 5 mm. The electrode lengths are 2 mm with a 0.5 mm gap between successive quadrupoles in the z direction.

Scintillator measurements of the beam exiting the structure show the expected quadrupole focusing effect. When all the quadrupoles are energized, the focused intensity is increased and the beam diameter is reduced. Faraday cup measurements also show that the transmitted current is more than doubled by the matching section. Experiments with the matching section coupled to the compact RF accelerator structure with four acceleration gaps (including two focusing quadrupoles between acceleration stages) showed Ar^+ ion acceleration ($\delta V > 2$ keV) from the additive acceleration from the four gaps.

The experience gained here point to improvements to the matching section design. Avoiding the warping caused by the nickel coating of the monomer electrode substrate may be accomplished by fabricating the part wholly out of metal in a 3D-printing process. Also, ports or vents on the side of the matching section will lower the local pressure in the path of the beam near the ion source, improving the voltage holdoff.

We are presently exploring methods for generating several kV of acceleration per acceleration gap with compact RF power sources. This is important to enable a compact accelerator (<1 m long) structure capable of generating 300 keV ions.

Higher average current and beam-power can be generated by introducing a bunching section[14] after the ion source and matching section to more efficiently capture (≈50%) the injected beam to the stable phase part of the RF acceleration waveform.

Scaling to many more parallel beams and higher current per beam will enable the development of this accelerator technology for high beam power applications. The fabrication and assembly costs scale favorably with these performance metrics. For example, for the 5-mm pitch between focusing channels tested here, there is ample space to increase the number of parallel beams to ≈160 on each 100-mm diameter wafer, while maintaining a low cost per wafer. Each beam could have a peak current of 120 μA, consistent with established current densities from plasma-based ion sources (ca. 15 mA/cm^2). A total beam current of >9 mA can be produced in a compact structure, for a total beam power in the kilowatt range.

ACKNOWLEDGMENTS

We thank Takeshi Katayanagi for excellent technical support. We are grateful for insightful discussions with Andris Faltens and James Galvin.

This work was supported by the US Department of Energy through the ARPA-E ALPHA program under Contract No. DE-AC0205CH11231.

[1] A. Persaud, Q. Ji, E. Feinberg, P. A. Seidl, W. L. Waldron, T. Schenkel, A. Lal, K. B. Vinayakumar, S. Ardanuc, and D. A. Hammer, Rev. Sci. Instrum. **88**, 063304 (2017).
[2] A. Persaud, P. A. Seidl, Q. Ji, E. Feinberg, W. L. Waldron, T. Schenkel, S. Ardanuc, K. B. Vinayakumar, and A. Lal, Phys. Procedia **90**, 136 (2017).
[3] A. Maschke, Technical Report BNL-51022, 1979.
[4] A. Maschke, Technical Report BNL-51029, 1979.
[5] W. Urbanus, R. Wojke, J. Bannenberg, H. Klein, A. Schempp, R. Thomae, T. Weis, and P. V. Amersfoort, Nucl. Instrum. Methods Phys. Res., Sect. B **37-38**, 508 (1989).
[6] R. O. Bangerter, A. Faltens, and P. A. Seidl, Rev. Accel. Sci. Technol. **06**, 85 (2013).
[7] *Industrial Accelerators and Their Applications*, edited by R. W. Hamm and M. E. Hamm (World Scientific, 2012).
[8] P. Sonato, P. Agostinetti, T. Bolzonella, F. Cismondi, U. Fantz, A. Fassina, T. Franke, I. Furno, C. Hopf, I. Jenkins, E. Sartori, M. Tran, J. Varje, P. Vincenzi, and L. Zanotto, Nucl. Fusion **57**, 056026 (2017).
[9] M. Reiser, *Theory and Design of Charged Particle Beams* (John Wiley and Sons, Inc., New York, 1994), Chap. 4, pp. 234–240.
[10] S. M. Lund, S. H. Chilton, and E. P. Lee, Phys. Rev. Spec. Top.–Accel. Beams **9**, 064201 (2006).
[11] R. Becker and W. B. Herrmannsfeldt, Rev. Sci. Instrum. **63**, 2756 (1992).
[12] See https://www.protolabs.com/media/638680/microfine-green-resin-fineline.pdf for "MicroFine Green Resin, ProtoLabs service."
[13] Q. Ji, P. Seidl, W. Waldron, J. Takakuwa, A. Friedman, D. Grote, A. Persaud, J. Barnard, and T. Schenkel, Rev. Sci. Instrum. **87**, 02B707 (2016).
[14] T. P. Wangler, *RF Linear Accelerators* (John Wiley and Sons, 2008), Chap. 4.